Author:	Taylor, Adam B.; Siddiquee, Arif M.; Chon, James W. M.
Title:	Below melting point photothermal reshaping of single gold nanorods driven by surface diffusion
Year:	2014
Journal:	ACS Nano
Volume:	8
Issue:	12
Pages:	12071-12079
URL:	http://hdl.handle.net/1959.3/393233
Copyright:	Copyright © 2014 American Chemical Society. This document is the unedited author's version of a submitted work that was subsequently accepted for publication in ACS Nano, copyright © American Chemical Society after peer review. To access the final edited and published work, see http://doi.org/10.1021/nn5055283

Below Melting Point Photothermal Reshaping Of Single Gold Nanorods Driven By Surface Diffusion

Adam B. Taylor[1], *Arif M. Siddiquee*[1] *and James W. M. Chon* [1]*

[1]Centre for Micro-Photonics, Faculty of Science, Engineering and Technology, Swinburne University of Technology PO Box 218 Hawthorn 3122 Victoria, Australia

KEYWORDS. Gold Nanorods, Photothermal Reshaping, Surface Diffusion, Plasmonics.

ABSTRACT. Plasmonic gold nanorod instability and reshaping behaviour at below melting points are important for many future applications but are yet to be fully understood, with existing nanoparticle melting theories unable to explain the observations. Here, we have systematically studied the photothermal reshaping behaviour of gold nanorods irradiated with femtosecond laser pulses to report that the instability is driven by curvature induced surface diffusion rather than threshold melting process, and that the stability dramatically decreases with increasing aspect ratio. We successfully utilized surface diffusion model to explain the observations and found that the activation energy for surface diffusion was dependent on the aspect ratio of the rods, from 0.6 *eV* for aspect ratio of 5, to 1.5 *eV* for aspect ratio less than 3. This result indicates that the surface atoms are much easier to diffuse around in larger aspect ratio rods than shorter rods, and can induce reshaping at any given temperature. Current plasmonics and nanorod applications with the sharp geometric features used for greater field enhancement will therefore need to consider surface diffusion driven shape change even at low temperatures.

The use of gold nanorods has become pervasive in many recent technological advancements including biolabelling, [1, 2] sensing, [3, 4] data storage, [5, 6] photovoltaics, [7-9] and cancer therapy. [10, 11] These techniques take advantage of the strong Localised Surface Plasmon Resonance (LSPR) inherent in the gold nanorods, and their stability is vital for preserving the LSPR and the success of these applications. [12-14] However, instability of the shape during laser exposure has been reported by many and reshaping of nanorods was observed to occur at temperatures as low as 400 K. [15-17] Petrova *et al*. and Liu *et al.* observed thermal reshaping of aspect ratio 3 gold nanorods at low temperatures [15, 17] when subjected to heat for extended period. Khalavka *et al.* reported [18] similarly low temperature shape transformation, but also reported enhancing the stability by coating thin carbon layer. Plech *et al.* [19] reported surface phase transition of gold nanoparticles at 400 K. Stability of gold nanorods during ultrafast pulsed laser irradiation is also of concern, due to unclear reshaping threshold and the high temperature that can be reached during irradiation. Yamaguchi's group reported low aspect ratio gold nanoparticle reshaping at 5.6 mJ/cm^2 for 30 ps pulsed laser, [20] while Zijlstra *et al.* [5, 21, 22] reported 1.125 to 1.75 mJ/cm^2 for 100 fs pulsed laser irradiation.

Typically, the melting point of nano-sized particles were predicted to be lower than bulk melting point, and observed by many. [23-28] Melting models such as homogeneous melting and growth model (HMG), [26, 27] liquid nucleation and growth (LNG), [23, 29] liquid shell nucleation (LSN), [30, 31] and liquid drop models [28] have been proposed for spherical particles. For nanorods or wires, thermodynamic modeling [24] and liquid-drop model [32] were proposed to explain the reduced melting points with respect to aspect ratios of nanorods. However, these models were unsuccessful in explaining the observed instability and reshaping of nanorods at temperatures as low as 400 K.

Molecular Dynamics simulations have been used to study melting behaviour of gold nanorods with size much less than 500k atoms. [33-36] Wang and Dellago studied nanosecond pulse heating on gold nanorods of size less than 10k atoms, to find lower melting points. [34, 35] Recently Gan and Jiang [36] extended the heating rate to femtosecond time scale using two-temperature model to match the recent experimental conditions of ultrafast laser exposures, which incorporates fast heat decay to the surrounding material. Surface melting was observed in these simulations. However the limitation in simulation time scales of MD simulation prohibits probing complete evolution of rod shapes in experimental time scale on the order of seconds. Typically the MD simulation focuses on the instantaneous structures during rapid heating which is far from the final structure that is being observed in microscopy.

Here, we report an experimental study on photothermal reshaping behaviour of gold nanorods to show that their reshaping can be initiated well below the melting points and are heavily dependent on aspect ratio. From this result we suggest curvature-driven surface diffusion, rather than threshold melting, to be the main physical mechanism for photothermal reshaping of gold nanorods. We successfully explain the observations with a theoretical framework of surface diffusion by Mullins. [37-39] Previously, Herring [40] and Nichols and Mullins [37, 41] used the curvature-driven surface diffusion to explain the blunting of microscopic objects such as sharp scanning tunnelling microscope tips, field emission guns, and sintering of metallic microspheres or smoothing of scratches on surfaces. More recently, Combe *et al.* [42] simulated the facet nucleation induced shape change of nanoclusters (of less than 13000 atoms) using surface diffusion Monte Carlo method. The surface diffusion framework shown in these works allow low temperature reshaping of gold nanorods without invoking the concept of low melting point. The time scales of previous reshaping experiments using constant temperature heating at low temperatures [15-17] were on the order of seconds and minutes, which is enough for surface diffusion to drive the shape change.

RESULTS AND DISCUSSION

Experimentally, we irradiated 600 randomly distributed and oriented gold nanorods (mean aspect ratio 3.5, average width 15.5 nm, from NanoSeedz) with linearly polarised, single femtosecond laser pulses (pulse width ~ 150 fs) at 830 nm wavelength with a typical fluence of 4.8 mJ / cm^2 to "angularly deplete" the nanorods. The random distribution in nanorod aspect ratio and orientation angle, relative to laser wavelength and polarization, creates natural variation in absorbed energies between each rod, enabling the reshaping behaviour to be extracted statistically, as a function of aspect ratio and absorbed energy. Further, excitation by ultrafast laser pulse induces temperature sweep of the nanorods, allowing extraction of diffusion coefficients over large temperature range rather than a single value. The activation energy for the diffusion could therefore be measured (Full experimental details are provided in Supporting Information section 1 Materials and Methods and Figures S1 – S7).

In Fig. 1a, selected rods oriented at particular angles to laser pulse polarization are shown before and after the pulse irradiation to illustrate the variation in their absorbed energy and their reshaping. Nanorods with long axes aligned close to the polarization angle exhibit reshaping after laser irradiation, while the reshaping is markedly less for orthogonally aligned nanorods, as expected for $\cos^2\theta$ relationship of absorbed energy. [21] A scatter plot showing the orientation angle and aspect ratio of individual nanorods before and after reshaping is shown in Fig. 1b, with the arrows indicating the vectors for reshaping trajectories. One might expect nanorods with aspect ratios and orientation angles resonant to the laser pulse wavelength and polarization (crossing point of the green lines) to show the largest magnitude of the vector and then it decreases as moving away from the resonance position on the plot. However such trend was not obvious from the figure. Instead, the nanorods with higher aspect ratios, *i.e.*, right side of the vertical green line, show drastic reshaping towards spheres despite their reduced absorption cross-sections at the laser wavelength, suggesting a decreasing thermodynamic stability with increasing aspect ratio.

This phenomenon is more clearly shown in Fig. 2, where the final aspect ratios of the nanorods for a tight range of aspect ratio bins (0.1 ~ 0.2) are plotted against the absorbed energy from a single pulse. In order to account for distribution in the constituent nanorods volume within each aspect ratio bin, the energy absorbed by each nanorod Q_{abs} is normalized by its mass m_{NR}, leading to the unit $q_{abs} = Q / m_{\mathrm{NR}}$, the absorbed energy per unit mass in J/g. The energy density required to reach the bulk melting point of gold q_{melt}^{bulk} was estimated to be 195 J/g (calculated using the Two-Temperature Model TTM with specific heat function of gold and heat loss, ie., , $q_{melt}^{bulk} = \int_{T_i}^{T_f} C_{gold}(T)dT + q_{loss}$ [43]) and that including the latent heat of fusion q_{final}^{bulk} , *i.e.*, $q_{final}^{bulk} = q_{melt}^{bulk} + (h_f + q_{loss})$ (~ 266 J/g), is shown in the figures as vertical lines. Examining Fig. 2, nanorods undergo a gradual shape transition below the melting point instead of abrupt reshaping at the vertical lines, which might be expected for threshold melting. This indicates that the reshaping is not driven by threshold melting. In order to accurately compare the results to the existing theories of nanostructure melting point suppression, the complete reshaping point, q_{final}^{expt} (*i.e.*, q for reaching final aspect ratio ~1) was extracted by fitting a simple quadratic function, ($AR_{\mathrm{final}} = AR_{\mathrm{initial}} - bq^2$) to the data points (fitting curves not shown).[44] Theoretical q_{final} ie.,

q_{final}^{theory} from previous models for infinite wire melting points, thermodynamic (TD) model [24] and liquid drop (LD) model [28] with correction for finite nanorod aspect ratio according to the equation by Goswami *et al.* [32] are calculated for average sizes in the binning ranges (see details of those calculations in Supporting Information 2). The values are shown in Fig. 2j and k, where the theory models only predict minimal variation for the rods used in this study. q_{final}^{expt} for initial aspect ratio range from 2.7 to 4 (Fig. 2a- 2e) follow more or less similar to the previous result [21], with the final reshaping to sphere occurring at the about 20 ~ 70 % above the energy density required to reach bulk melting point and latent heat of fusion. However, as the aspect ratio increases (Figs. 2f - 2i), the q_{final}^{expt} decreases dramatically, from 350 J/g for AR 3.6, to 150 J/g for AR 4.9. It is evident that for aspect ratios beyond 4, q_{final}^{expt} is well below that required for reaching melting point.

Such below melting point reshaping indicates that the existing theories for melting point of nanorods are not sufficient to explain the observed results. Since the change in aspect ratio below melting point has to involve mass diffusion and the nanorod surface has a large change in curvature from tip to the waist, the curvature driven surface diffusion is the likely driving mechanism for the observed reshaping.

Previously, Mullins [37-39] proposed a theory on the curvature driven reshaping and successfully explained the blunting of field emission gun tips in electron microscope or scanning tunneling microscope tips below melting point. The central idea of this theory is the surface diffusion acting to minimize the surface energy of an object. The surface flux of diffusing atoms $\mathbf{J}_s$ can be expressed by

$$\mathbf{J}_s = \frac{\Omega v_s}{kT} \overleftrightarrow{\mathbf{D}}_s \cdot \nabla \mu \qquad (1)$$

where Ω is an atomic volume, v_s is the number of diffusing surface atoms in the unit area, k is the Boltzman's constant, T is temperature, and μ is the chemical potential. $\overleftrightarrow{\mathbf{D}}_s$ is the interface diffusivity tensor. The gradient notation ∇ is two-dimensional on the surface. Eq. (1) should satisfy the equation of continuity, $\frac{\partial n}{\partial t} + \nabla \cdot \mathbf{J}_s = 0$ where $\partial n / \partial t$ represents the movement speed of a point on the surface in the outward normal direction to the surface. For an isotropic surface, the diffusivity tensor can be simplified as $D_s(T)$, with typical Arrhenius behaviour with an activation energy E_a and a constant D_0 as

$$D_s(T) = D_0 \exp\left(\frac{-E_a}{kT}\right). \qquad (2)$$

The chemical potential μ can also be simplified for an isotropic surface, following the Herring's formula, [37, 40]

$$\mu = \mu_0 + \gamma_s \Omega K \qquad (3)$$

where $K = 1/R_x + 1/R_y$ is the mean curvature of the surface and γ_s is the free energy, and μ_0 is the chemical potential for a flat surface. The Eq. 1 becomes

$$\frac{dn}{dt} = v = B\nabla^2 K, \qquad (4)$$

where $B = \frac{\Omega^{4/3} \gamma_s D_s}{kT}$. The equation relates the movement speed of a surface point to the curvature driven surface diffusion.

The finite difference method [37] can be applied to the Eq. 4 to simulate the reshaping behaviour. Movement of points on the entire surface of a nanorod is calculated using Eq. 4 for each time step $t = t_i$, to account for surface motion at given temperature T. Fig. 3a shows a reshaping evolution of an ellipsoidal nanorod (15 x 50 nm) subjected to a fixed temperature (430 K), which is an identical experimental condition that Liu *et al.* have previously shown. [17] We have therefore overlaid Liu *et al.*'s data on our curve. One could see the gradual migration of atoms with respect to the time, from the high curvature, *i.e.*, tip, to the low curvature, *i.e.*, waist of the rods. Good fit with the experimental results by Liu *et al.* shows that the theory accurately accounts the reshaping behaviour at low temperatures. We have also independently fitted results by Petrova *et al.* [15] and Tollan *et al.*, [16] which used oven or heating stage to induce thermal reshaping of aspect ratio ~ 3.3 gold nanorods. The fitting parameter for these results revealed that the D_s varied between 10^{-10} to 10^{-15} cm^2/s depending on their temperature. This matches well with previously observed values for nanostructured gold surfaces. [45]

In photothermal reshaping using ultrafast pulsed laser irradiation, the temperature sweeps from room temperature to potentially above melting points in a picosecond time scale. In order to account for the temperature sweep in such a short time scale, we employed two-temperature model [43] (full details of TTM calculations are included in the Supporting Information 3) to calculate the temperature profile $T(t_i)$ of gold nanorod during an ultrashort pulse irradiation. The fast temperature change with time steps on the order of 0.1 ps to 1 ps is accounted for in the $T(t_i)$ and it was input into Eq. 4 to simulate the reshaping evolution. The diffusion coefficient $D_s(T)$ is also a function of temperature, hence at each time step, the D_s value is obtained from the temperature $T(t_i)$ *via* the Arrhenius relation given by Eq. 2, with the activation energy, E_a and the prefactor D_0 used as fitting parameters.

A simulation of photothermal reshaping of a longer nanorod (AR 4.5), under ultrashort pulsed irradiation is shown in the Fig. 3b for fixed values of E_a, and prefactor D_0. The temperature profile is calculated using the TTM, with finite thermal conductance of the gold nanorod surface and surrounding polyvinyl alcohol accounted for. One could notice that due to the fast temperature decay, the nanorod does not fully reshape into sphere, but rather "freezes" at final aspect ratio of 1.7. This final value will obviously be dependent on absorbed energy density q_{abs}, and therefore the observed reshaping into lower aspect ratio rods in Fig. 2 can be accounted for using this theory.

This simulation technique was applied to fitting the observed reshaping of gold nanorods in Fig. 2. By using Eq. 4 and E_a and D_0 as fitting factors, we evolved the nanorod shape in time to observe the final aspect ratio after no change was observed. Typically the temperature falls back to room temperature within 10 ns, and reshaping slows to an undetectable rate. This provided a point in the Fig. 2, which plots the final reshaped aspect ratio AR_{final} against the absorbed energy, q_{abs}. This process was repeated by varying the pulse energy fluence F to obtain a complete curve for a single aspect ratio rod.

For comparison, we independently modeled the experimental conditions used by Liu *et al.* [17] in their experiment to extract the activation energy E_a and D_0 for AR 3.3 using the Eq. 4. We chose Liu's results because their nanorods have similar sizes to the ones that we have used in the current study. We then used these values to fit experimental data for our rods. The D_0 value of 40000 cm^2/s extracted from Liu *et al.*'s result were then used for other aspect ratio rods, assuming that at infinitely high temperature (*i.e.*, 1/T ~ 0) the value should not be different for different aspect ratio. This allowed only E_a as a fitting factor with respect to the initial aspect ratio of nanorods, *i.e.*, $E_a(AR_{\text{initial}})$.

Other conditions for E_a during the fitting was that 1) if the temperature hits the bulk melting point, the diffusion coefficient would show a sudden jump to account for the latent heat of fusion, as observed by MD simulations, [46, 47] 2) if the temperature overcomes the melting point, *i.e.*, $q_{abs} > q_{\mathrm{melt}} + h_f$, the activation energy would be reduced to account for the liquid phase of matter, and 3) D_0 is allowed to vary during the reshaping to account for increase in defects during reshaping. This was expressed according to the equation $D_0 = 40000\exp(\Delta S_D / k)$ where ΔS_D is the change in the entropy in diffusion.[48] This is assumed to increase linearly on the change in aspect ratio due to amorphous configuration reached during reshaping.

Simulated theory lines with upper and lower fit bounds are shown in Fig. 2 as solid lines, which show good agreements with the experimental points. The theory also accurately accounts for the reshaping behaviour of nanorods with AR > 4, where the reshaping takes place at q_{final} values well below that are required to reach melting point. The reduced X^2 of the surface diffusion model is plotted for the aspect ratio bins, along with that of threshold model[44] based on TD/LD melting models for a comparison (Supporting Information 4, Fig. S7). The X^2 is clearly superior for surface diffusion model compared to threshold models.

The values of the parameters D_s (T) lines and E_a (AR_{initial}) used for fitting individual AR values are shown in Fig. 4. All the D_s (T) lines (Fig.4a) show discontinuity at T= 1337 K, to account for the latent heat of fusion. The D_s (T) line for average AR 3.3 rods shows very good agreement with Liu *et al.*'s data (open circles). The activation energies needed to fit the experimental data (Fig. 4b) show higher values for shorter aspect ratios. At AR 2.7, E_a is 1.45 eV, and then it decreases to 0.6 eV as the AR increases past 4.7. This means that for higher aspect ratio rods, the energy barrier to overcome for surface atoms on the nanorods to be mobile and diffusive is much lowered, leading to easy reshaping well below melting point. This also explains in Fig. 2j why the shorter aspect ratio (AR<4) rods have q_{final} well above those of the longer ones, therefore appearing to be "more difficult" to reshape than longer ones.

Independent to the surface diffusion model, predicting the activation energy trend for nanorods require boundary conditions that E_a at AR ~ 1 (sphere) should be a finite value and E_a at AR ~ ∞, should converge to zero. A linear fit line fails to meet this condition, as it predicts a physically untenable negative value of E_a. Previously, the activation energy for below melting point nucleation of crystal facets due to surface diffusion was predicted to follow $E_a \sim 1/K$. [42] In terms of the dimensions of the rods, the $E_a \sim 1/K$ curve has the following expression,

$$E_a = \frac{2aC}{\left(AR^2 + 1\right)} \quad (5)$$

where a is the half of nanorod length and C is a constant of proportionality (refer to Supporting Information (5) for the derivation). Applying a similar argument, $E_a \sim 1/K$ curve for ellipsoidal nanorods is overlaid on Fig. 4b. The trend is in a reasonable agreement with the experimental results, with extracted value of C from Fig. 4b is $C = 2.6 \times 10^8 \frac{eV}{m}$. It is noted that the curvature K is dependent both on the aspect ratio the dimensions of the rod (a in this case). Therefore the aspect ratio dependencies of both curvature K and activation energy E_a has to be understood within the specified size regime.

Slightly larger E_a values (maximum ~ 20% at AR ~ 3.5) than the trend is observed below AR < 4. This may be due to shape deviation from prolate spheroids to paraboloidally or hemispherically capped cylinders, which reduces the curvature around the tip and therefore increasing E_a. This shape deviation should converge to the prolate spheroids for longer aspect ratio rods, as it is observed in Fig. 4b. Other potential source of error is the local temperature gradient within a single nanorod induced by strong plasmon field, which would affect the chemical potential and therefore could disturb purely curvature driven diffusion.

The absolute values of E_a are in good agreement with previous values in the literature. The reduced dimensions generally show reduced activation energy, at 1 ~ 1.5 eV for 40 ~ 50 nm thick gold films that show capillary induced instability, [49] with recent study shows the E_a less than 0.1 eV for ultrathin gold films (1 – 5 nm thick). [50] Activation energy for gold atomic steps are also shown to be in the range of 0.1- 0.8 eV, [48] and for spherical gold nanoparticles of diameter less than 5 nm show 0.54 eV. [51] With nanorod width ranging in between 10 – 20 nm with many crystallographic facets it is reasonable to observe the value in between the published data.

Finally, we discuss the role of chemical potential in surface diffusion based reshaping and its interface with purely melting based reshaping. While the current surface diffusion model accounts for melting based reshaping by sudden increase in diffusion coefficient in the $D_s(T)$ at melting points, it does not differentiate melting based reshaping to purely surface diffusion driven reshaping. Furthermore, the current model does not account for surface diffusion by local surface melting, which may exist due to the different surface energies of crystal facets, [33-35] or local temperature gradient, which may exist due to field enhancement at the tip during surface plasmon resonance. [52] To account for such complex situations chemical potential must be rigorously treated.

The chemical potential expression used in this manuscript ($\mu = \mu_0 + \gamma_s \Omega K$) has two terms. [37] First term μ_0 is for a flat surface and effectively contains all the temperature, pressure and phase dependencies [53, 54] (melting would be manifested in the phase differences). The second term is for a dependency with curvature only. The current formalism therefore do not take into account the surface diffusion due to spatial chemical potential gradients of temperature, pressure or phase differences. Strong field enhancements at the tip of rods, [52] acoustic vibrations [55] and patchy surface premelting [36] could all contribute to spatial gradients dependent on these parameters. If these gradients are assumed to exist within a nanorod, then the full expression for chemical potential is

$$\mu = \mu_T + \mu_{pr} + \mu_{ph} + \gamma_s \Omega K \qquad (6)$$

and accordingly, Eq. 4 is now modified to incorporate the spatial gradients of these parameters,

$$\frac{dn}{dt} = v = B_T \nabla^2 \mu_T + B_{pr} \nabla^2 \mu_{pr} + B_{ph} \nabla^2 \mu_{ph} + B_K \nabla^2 K \qquad (7)$$

where B is the constant of proportionality and subscript T, pr, and ph stands for their dependence on temperature, pressure and phase differences respectively.

Determining individual components experimentally is beyond the scope of this paper. Perhaps variable temperature electron microscopy could be used to detect a sudden change in reshaping behaviour near melting point, and the terms μ_{ph} and B_{ph} might potentially be measured. In this case, phase change (*i.e.*, melting) based reshaping process could be decoupled from surface diffusion based reshaping.

Proposed experimental work could also explain why the complete reshaping energy q_{final} at certain aspect ratio of nanorods appears to match the existing theoretical melting models (*i.e.*, AR 2.8 in Fig. 2j,) better than others. We speculate that the amount of nanorod mass that has to be shifted to reshape into spheres plays important role in explaining the apparent agreement with existing models at certain aspect ratios. For example, an aspect ratio 2.8 nanoparticle have 28% less mass to shift than the 3.5 nanorods to reshape to an aspect ratio 1 sphere. Here then two opposing processes exist, faster rates of diffusion for increasing aspect ratios, but increasing amounts of mass which have to diffuse for these increased aspect ratios to reshape to spheres. There might be a crossing point for these two competing processes.

Study of these two competing effect will require detailed experimental study into shorter aspect ratios (1 ~ 3). Further, in order to remove the bias towards specific nanorod population selection by exciting at longitudinal SPR band of nanorods, a transverse SPR could be excited (at ~ 530 nm) instead, where all the rods have absorption.

CONCLUSION

In conclusion, we have shown that the thermal stability of gold nanorods dramatically decreases with increasing aspect ratio, and that reshaping can occur far below the bulk melting temperature for higher aspect ratios. We successfully explained the observation with surface diffusion on the nanorods, resulting from the increased surface curvature of the higher aspect ratio nanorods. The activation energy for the surface diffusion were found to be dependent on the aspect ratio, with values ranging from 0.6 ~ 1.5 eV. These findings will be especially important for the field of gold nanorod photothermal therapy and two-photon biolabelling, plasmonic circuitry, solar cells using plasmonic structure, [1-4, 7-11, 14] where increased laser power, and sharper geometric features are often seen as a mechanism for greater field enhancement. This work shows that surface diffusion based reshaping must be considered for plasmonic nanostructures for their stable operations, even at temperatures well below melting points.

METHODS

Gold nanorods were purchased from Nanoseedz (NR-20-750) which has average aspect ratio of 3.5 (standard deviation 0.5) with average width 15.5 nm. From transmission electron microscope (TEM) images, we could observe aspect ratio ranging from 2.7 ~ 5, which is of interest to most applications. The nanorod solution was mixed with polyvinyl alcohol (PVA) and was centrifuged on a TEM grid, before the TEM imaging. Once the imaging is completed, the grid is transferred to optical set up for laser irradiation.

The experimental setup for laser irradiation is shown in Fig. S1. Single femtosecond laser pulses from a Ti-Sapphire laser (Tsunami, Spectra-Physics) are picked using a pulse picker (Conoptics), and then focused on the sample using 1.4 numerical aperture, oil-immersion objective lens (Olympus). The sample is mounted onto a piezo stage for scanning. The 2D lattice of points used for heating is shown in Fig. S2. The exposure was controlled using a LabView, where a piezo stage moves the sample so that the shaded area was aligned with the full width at half maximum (FWHM) focal spot of the 1.4 NA objective. This sample was again shifted, and the process was repeated until the entire sample area was exposed.

Laser scattering image is built up by confocal detection or back-scattered photons from nanorods using a photomultiplier tube (PMT, Oriel) and the scattering cross sections σ_{scat}^{meas} for rods were extracted (Fig. S3). Absorption cross sections of individual rods σ_{abs}^{meas} at 830 nm were estimated from the measured scattering cross sections σ_{scat}^{meas} using the equation, $\sigma_{abs}^{meas}(\lambda = 830nm) = \sigma_{scat}^{meas}(\lambda = 830nm) \times \sigma_{abs}^{theory} / \sigma_{scat}^{theory}$. The σ_{abs}^{meas} for ~ 600 nanorods are plotted in the Fig. S4 with theoretical absorption cross sections.

The variation in aspect ratio and orientation allowed variation in energy absorption per nanorods according to the equation $Q = \sigma_{abs} I \cos^2\theta$, where θ is the angle between the polarization and rod orientation, and subsequent photothermal reshaping. We imaged rods at single particle level using TEM before and after the linearly polarized laser irradiation to observe their reshaping behaviour. The geometry before and after reshaping is determined with the assistance of London Finder TEM grids, which use an alpha-numeric co-ordinate marked system to locate the same area. To extract the geometric dimensions of the gold nanorods, we use the software package ImageJ, using the 'Fit Ellipse' option to fit an ellipse around each particle and thus extract the length, width, and orientation angle. Typical wide area TEM micro-graphs are shown in Fig. S5, with before and after laser irradiation images. A distribution in the length and widths of the 600 observed nanorods before reshaping is shown in Fig. S6. A scatter plot showing the lengths and widths of the observed nanorods before and after melting is shown in Fig. S7.

FIGURES

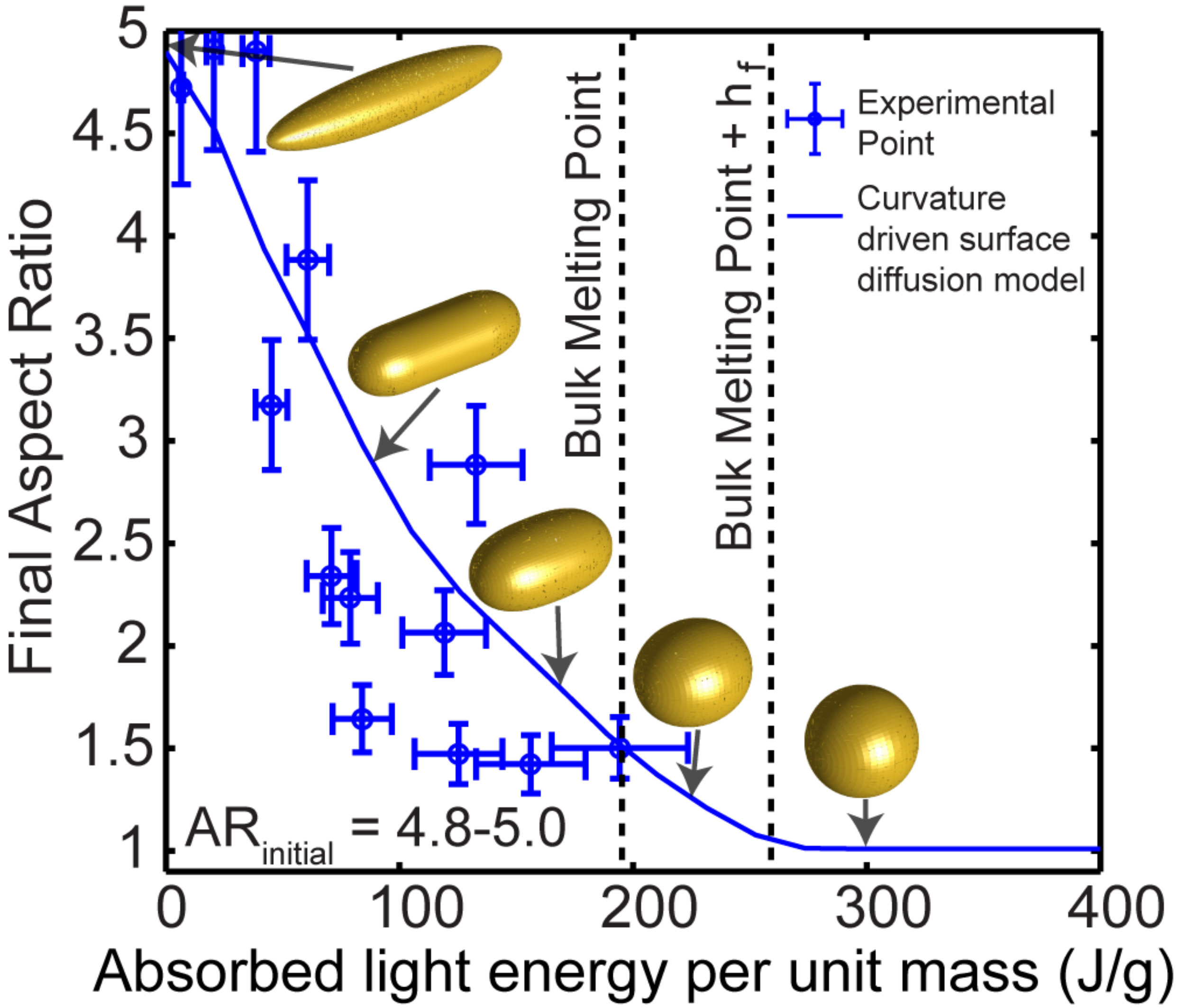

TOC Figure: Photothermal reshaping of gold nanorods below melting points driven by surface diffusion.

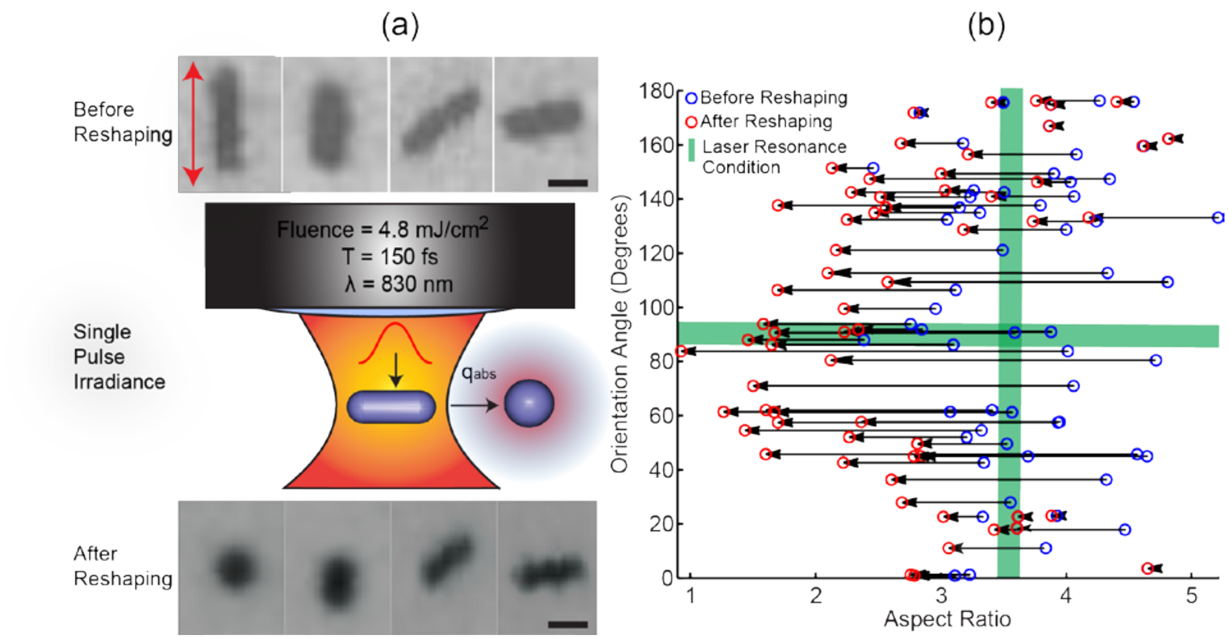

Figure 1. (a) Schematic showing the angular depletion method of photothermal reshaping: Nanorods are imaged on a co-ordinate marked TEM slide in a precise location, then a single pulse is applied to all the nanorods to heat and reshape them, and finally the same rods are located and imaged again to quantify the degree of reshaping. TEM imaged of the same nanorods before and after single pulse excitation with vertically polarized light. Scale bar is 20 nm. Note that as the orientation misalignment increases, the reshaping becomes less. (b) A vector plot showing reshaping trajectories of individual nanorods after laser pulse irradiation. Green lines show resonant rod aspect ratio/orientation with laser condition, ie., 830 nm wavelength and 90° polarization.

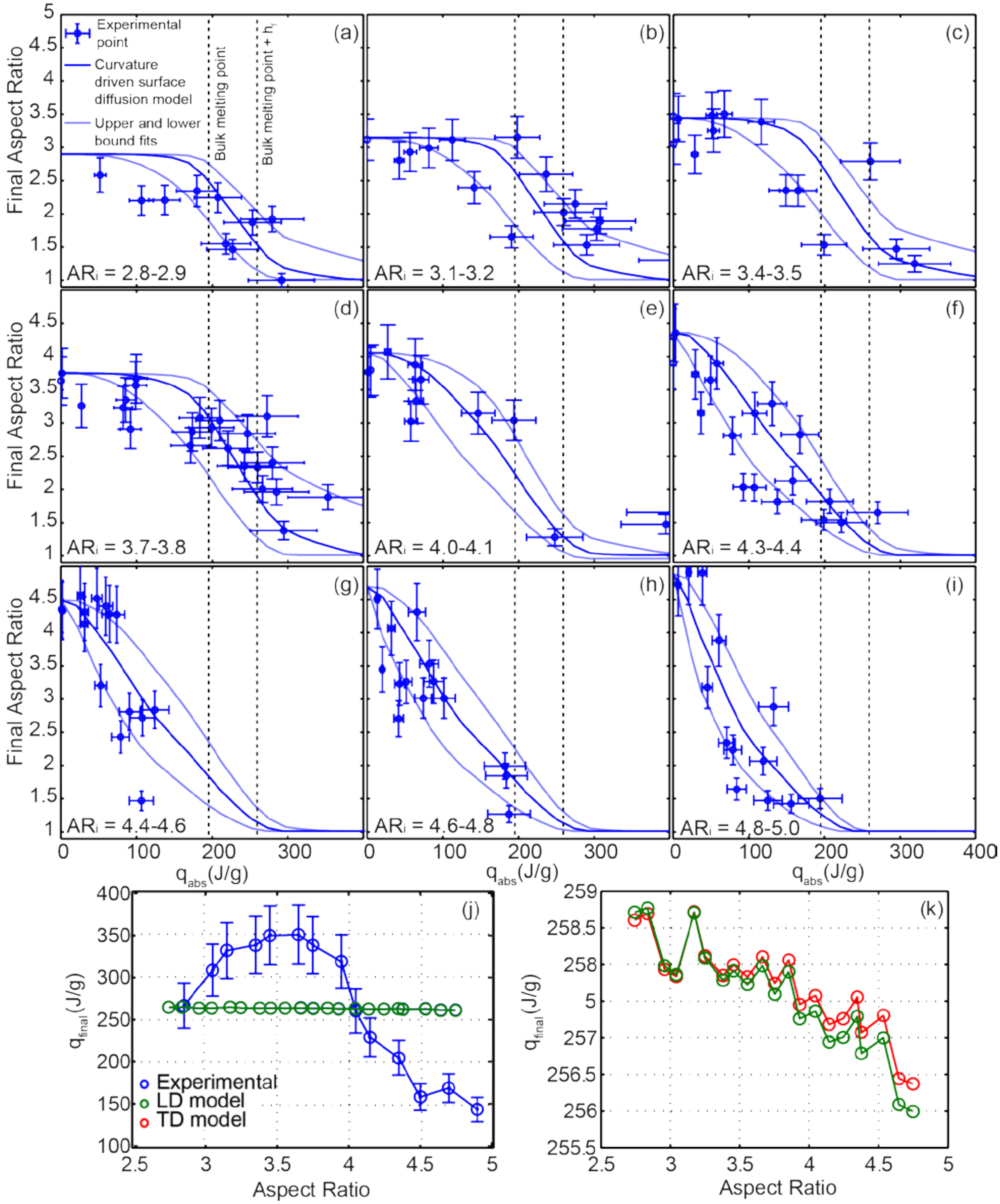

Experimental point
Curvature driven surface diffusion model
Upper and lower bound fits
Bulk melting point
Bulk melting point + h_f
Final Aspect Ratio
(a)
(b)
(c)
(d)
(e)
(f)
(g)
(h)
(i)
ARi = 2.8-2.9
ARi = 3.1-3.2
ARi = 3.4-3.5
ARi = 3.7-3.8
ARi = 4.0-4.1
ARi = 4.3-4.4
ARi = 4.4-4.6
ARi = 4.6-4.8
ARi = 4.8-5.0
q_abs(J/g)
(j)
(k)
q_final(J/g)
Experimental
LD model
TD model
Aspect Ratio

Figure 2. (a-i) Photothermal reshaping behaviour of gold nanorods in respective aspect ratio range bins. Final aspect ratio vs absorbed energy density q_{abs}. Aspect ratio ranges from 2.7 to 5.0. Points with error bars are experimental results. Solid blue lines are the theoretical simulation using the Eq. 1 – 4, see text. The two vertical lines indicate the energy density needed to reach the melting temperature, and to overcome the latent heat of fusion h_f. (j) The complete reshaping point q_{final} vs the aspect ratio extracted from the figures a-i. Black and red lines are the existing theoretical complete reshaping points, ie., q_{final}^{theory}. Thermodynamic (TD) model [24] and liquid-drop (LD) model [28, 32] calculated for average aspect ratio and volume of the nanorods within each bin. (k) Close-up view of theory lines of q_{final}^{theory} values showing only a small change around 255 J/g.

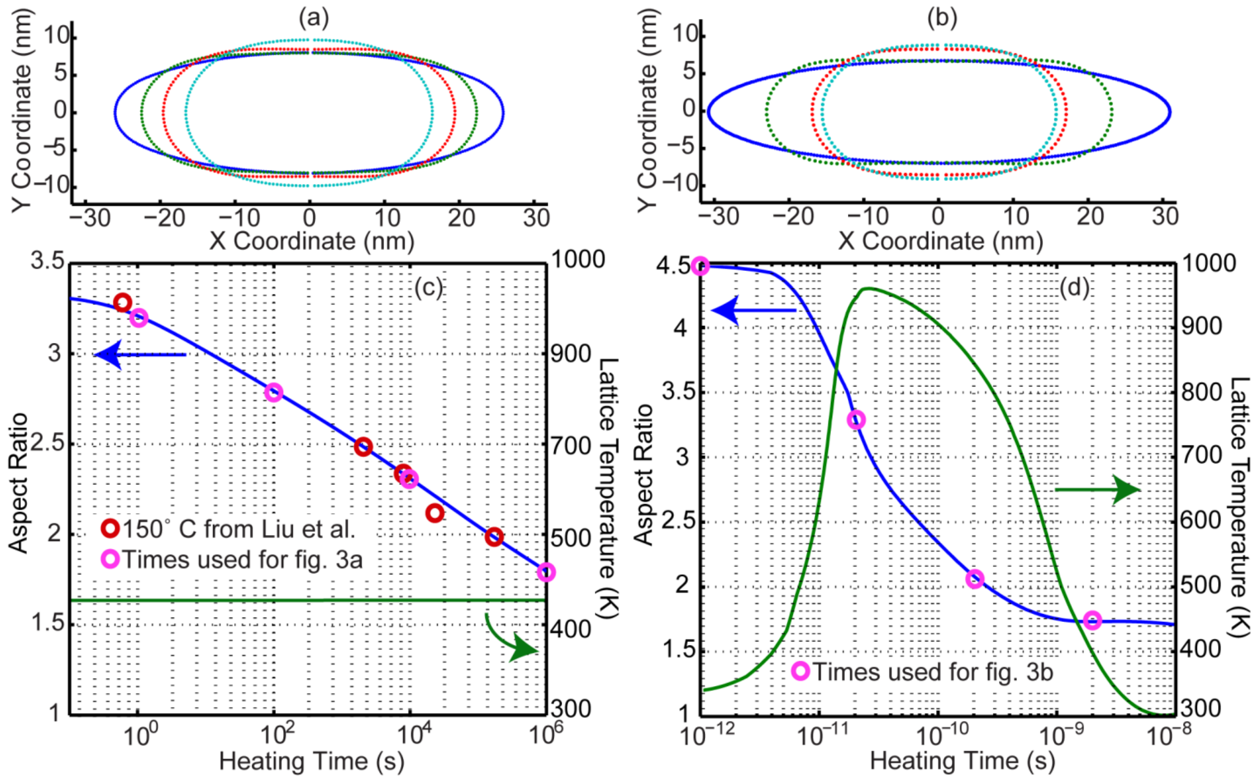

Figure 3. Simulated shape evolution of nanorods with aspect ratio 3.3 (a) for constant temperature at 430 K (~ 150° C) for various times showing the reshaping trajectory. (c) Reshaping trajectory with respect to time (blue line) and the temperature is shown as green line. Data by Liu *et al.* [17] are shown as red circles and show good agreement with the trajectory. The D_s = 2.12 x 10^{-12} cm^2/s was revealed from the fit. (b) Shape evolution of aspect ratio 4.5 rod by a pulsed laser irradiation (150 fs pulse width). (d) Reshaping trajectory (blue line) and the temperature sweep profile, calculated using the TTM (see Supplemental Information 3), and the reshaping profiles were calculated using Eq. 4. The activation energy E_a for the D_s (T) curve was 1.32 eV.

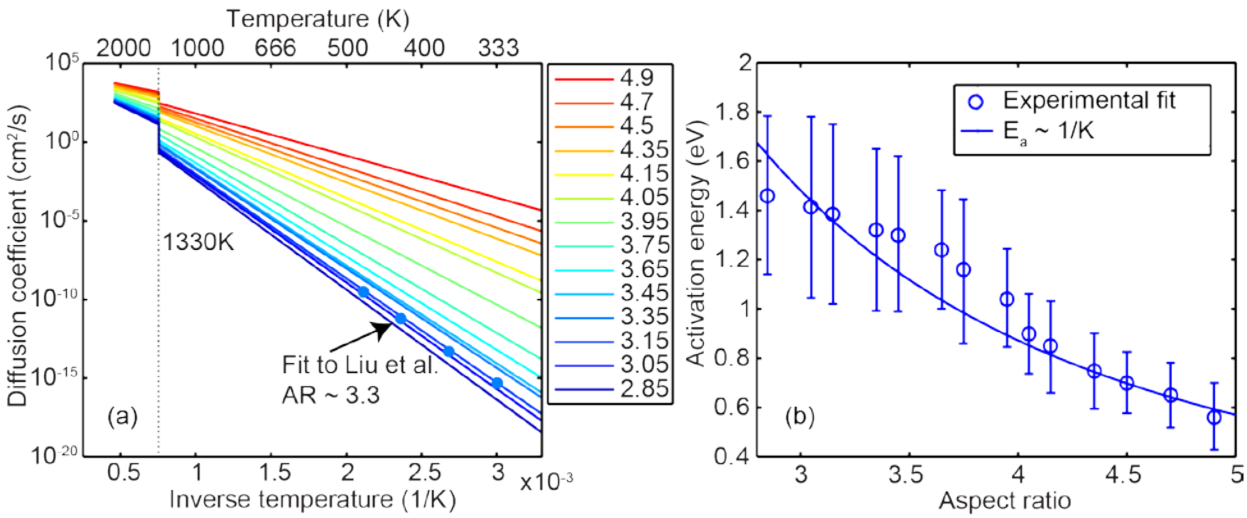

Figure 4. (a) Temperature dependent surface diffusion coefficients D_s (T) used for the theoretical fitting with Eq. 3 to the experimental data for a range of initial aspect ratios. The points indicate the diffusion coefficients used to fit Liu *et al.*'s experimental results. [17] (b) The activation energies used for the best fit to the experimental points in Fig. 2. Overlaid is the ~ $1/K$ activation energy relation with respect to aspect ratio, where K is the tip curvature.

ASSOCIATED CONTENT

Supporting Information. Supporting information on detailed experimental methods, (Figures S1-S8), nanorod melting theories and two-temperature model is provided. This material is available free of charge *via* the Internet at http://pubs.acs.org.

AUTHOR INFORMATION

Corresponding Author

* Correspondence should be addressed to James W. M. Chon jchon@swin.edu.au.

Author Contributions

The manuscript was written through contributions of all authors. All authors have given approval to the final version of the manuscript.

Funding Sources

Australian Research Council, funding ID FT110101038 and DP110102870

ACKNOWLEDGMENT

Authors would like to thank the Australian Research Council for the funding of the research, with funding ID FT110101038 and DP110102870.

REFERENCES

1. Durr, N. J.; Larson, T.; Smith, D. K.; Korgel, B. A.; Sokolov, K.; Ben-Yakar, A. Two-Photon Luminescence Imaging of Cancer Cells Using Molecularly Targeted Gold Nanorods. *Nano Lett.* **2007,** 7, 941-945.
2. Wang, H.; Huff, T. B.; Zweifel, D. A.; He, W.; Low, P. S.; Wei, A.; Cheng, J. X. Controlling the Cellular Uptake of Gold Nanorods. *Proc. Natl. Acad. Sci. U. S. A.* **2005,** 102, 15752-15756.
3. Yu, K.; Zijlstra, P.; Sader, J. E.; Xu, Q. H.; Orrit, M. Damping of Acoustic Vibrations of Immobilized Single Gold Nanorods in Different Environments. *Nano Lett.* **2013,** 13, 2710-2716.

4. Yuan, H. F.; Khatua, S.; Zijlstra, P.; Yorulmaz, M.; Orrit, M. Thousand-Fold Enhancement of Single-Molecule Fluorescence Near a Single Gold Nanorod. *Angew. Chem. Int. Ed.* **2013,** 52, 1217-1221.
5. Zijlstra, P.; Chon, J. W. M.; Gu, M. Five-Dimensional Optical Recording Mediated by Surface Plasmons In Gold Nanorods. *Nature* **2009,** 459, 410-413.
6. Chon, J. W. M.; Bullen, C.; Zijlstra, P.; Gu, M. Spectral Encoding on Gold Nanorods Doped in a Silica Sol–Gel Matrix and its Application to High-Density Optical Data Storage. *Adv. Funct. Mater.* **2007,** 17, 875-880.
7. Schuller, J. A.; Barnard, E. S.; Cai, W. S.; Jun, Y. C.; White, J. S.; Brongersma, M. L. Plasmonics for Extreme Light Concentration and Manipulation. *Nat. Mater.* **2010,** 9, 193-204.
8. Mubeen, S.; Lee, J.; Singh, N.; Kramer, S.; Stucky, G. D.; Moskovits, M. An Autonomous Photosynthetic Device in which all Charge Carriers Derive from Surface Plasmons. *Nat. Nanotechnol.* **2013,** 8, 247-251.
9. Atwater, H. A.; Polman, A. Plasmonics for Improved Photovoltaic Devices. *Nat. Mater.* **2010,** 9, 205-213.
10. Huang, X.; El-Sayed, I. H.; Qian, W.; El-Sayed, M. A. Cancer Cell Imaging and Photothermal Therapy in the Near-Infrared Region by Using Gold Nanorods. *J. Am. Chem. Soc.* **2006,** 128, 2115-2120.
11. Choi, W. I.; Sahu, A.; Kim, Y. H.; Tae, G. Photothermal Cancer Therapy and Imaging Based on Gold Nanorods. *Ann. Biomed. Eng.* **2012,** 40, 534-46.
12. Ungureanu, C.; Kroes, R.; Petersen, W.; Groothuis, T. A. M.; Ungureanu, F.; Janssen, H.; van Leeuwen, F. W. B.; Kooyman, R. P. H.; Manohar, S.; van Leeuwen, T. G. Light Interactions with Gold Nanorods and Cells: Implications for Photothermal Nanotherapeutics. *Nano Lett.* **2011,** 11, 1887-1894.
13. Yoon, S. J.; Murthy, A.; Johnston, K. P.; Sokolov, K. V.; Emelianov, S. Y. Thermal Stability of Biodegradable Plasmonic Nanoclusters in Photoacoustic Imaging. *Opt. Express* **2012,** 20, 29479-29487.
14. Joy, N. A.; Janiszewski, B. K.; Novak, S.; Johnson, T. W.; Oh, S. H.; Raghunathan, A.; Hartley, J.; Carpenter, M. A. Thermal Stability of Gold Nanorods for High-Temperature Plasmonic Sensing. *J. Phys. Chem. C* **2013,** 117, 11718-11724.
15. Petrova, H.; Juste, J. P.; Pastoriza-Santos, I.; Hartland, G. V.; Liz-Marzán, L. M.; Mulvaney, P. On the Temperature Stability of Gold Nanorods: Comparison Between Thermal and Ultrafast Laser-Induced Heating. *Phys. Chem. Chem. Phys.* **2006,** 8, 814-821.
16. Tollan, C. M.; Marcilla, R.; Pomposo, J. A.; Rodriguez, J.; Aizpurua, J.; Molina, J.; Mecerreyes, D. Irreversible Thermochromic Behavior in Gold and Silver Nanorod/Polymeric Ionic Liquid Nanocomposite Films. *ACS Appl. Mater. Interfaces* **2009,** 1, 348-352.
17. Liu, Y.; Mills, E. N.; Composto, R. J. Tuning Optical Properties of Gold Nanorods in Polymer Films through Thermal Reshaping. *J. Mater. Chem.* **2009,** 19, 2704-2709.
18. Khalavka, Y.; Ohm, C.; Sun, L.; Banhart, F.; Sonnichsen, C. Enhanced Thermal Stability of Gold and Silver Nanorods by Thin Surface Layers. *J. Phys. Chem. C* **2007,** 111, 12886-12889.
19. Plech, A.; Cerna, R.; Kotaidis, V.; Hudert, F.; Bartels, A.; Dekorsy, T. A Surface Phase Transition of Supported Gold Nanoparticles. *Nano Lett.* **2007,** 7, 1026-1031.
20. Inasawa, S.; Sugiyama, M.; Yamaguchi, Y. Laser-Induced Shape Transformation of Gold Nanoparticles Below the Melting Point: the Effect of Surface Melting. *J. Phys. Chem. B* **2005,** 109, 3104-3111.

21. Zijlstra, P.; Chon, J. W. M.; Gu, M. White Light Scattering Spectroscopy and Electron Microscopy of Laser Induced Melting in Single Gold Nanorods. *Phys. Chem. Chem. Phys.* **2009,** 11, 5915-5921.
22. Zijlstra, P.; Chon, J. W. M.; Gu, M. Effect of Heat Accumulation on the Dynamic Range of a Gold Nanorod Doped Polymer Nanocomposite for Optical Laser Writing And Patterning. *Opt. Express* **2007,** 15, 12151-12160.
23. Couchman, P. R.; Jesser, W. A. Thermodynamic Theory of Size Dependence of Melting Temperature in Metals. *Nature* **1977,** 269, 481-483.
24. Gülseren, O.; Ercolessi, F.; Tosatti, E. Premelting of Thin Wires. *Phys. Rev. B* **1995,** 51, 7377-7380.
25. Hoss, A.; Nold, M.; Von Blanckenhagen, P.; Meyer, O. Roughening and Melting of Au(110) Surfaces. *Phys. Rev. B* **1992,** 45, 8714-8720.
26. Buffat, P.; Borel, J. P. Size Effect on the Melting Temperature of Gold Particles. *Phys. Rev. A* **1976,** 13, 2287-2298.
27. Pawlow, P. The Vapour Pressure of Grains of a Solid Substance. *Zeitschrift Fur Physikalische Chemie--Stochiometrie Und Verwandtschaftslehre* **1909,** 65, 545-548.
28. Nanda, K. K.; Sahu, S. N.; Behera, S. N. Liquid-Drop Model for the Size-Dependent Melting of Low-Dimensional Systems. *Phys. Rev. A: At., Mol., Opt. Phys.* **2002,** 66, 132081-132088.
29. Reiss, H.; Mirabel, P.; Whetten, R. L. Capillarity Theory for the" Coexistence" of Liquid and Solid Clusters. *J. Phys. Chem.* **1988,** 92, 7241-7246.
30. Sakai, H. Surface-Induced Melting of Small Particles. *Surf. Sci.* **1996,** 351, 285-291.
31. Hoss, A.; Nold, M.; Vonblanckenhagen, P.; Meyer, O. Roughening and Melting of Au(110) Surfaces. *Phys. Rev. B* **1992,** 45, 8714-8720.
32. Goswami, G. K.; Nanda, K. K. Size-Dependent Melting of Finite-Length Nanowires. *J. Phys. Chem. C* **2010,** 114, 14327-14331.
33. Opletal, G.; Grochola, G.; Chui, Y. H.; Snook, I. K.; Russo, S. P. Stability and Transformations of Heated Gold Nanorods. *J. Phys. Chem. C* **2011,** 115, 4375-4380.
34. Wang, Y.; Dellago, C. Structural and Morphological Transitions in Gold Nanorods: a Computer Simulation Study. *J. Phys. Chem. B* **2003,** 107, 9214-9219.
35. Wang, Y.; Teitel, S.; Dellago, C. Surface-Driven Bulk Reorganization of Gold Nanorods. *Nano Lett.* **2005,** 5, 2174-2178.
36. Gan, Y.; Jiang, S. Ultrafast Laser-Induced Premelting and Structural Transformation of Gold Nanorod. *J. Appl. Phys.* **2013,** 113, 073507.
37. Nichols, F. A.; Mullins, W. W. Morphological Changes of a Surface of Revolution due to Capillarity-Induced Surface Diffusion. *J. Appl. Phys.* **1965,** 36, 1826-1835.
38. Mullins, W. W. Mass-Transport at Interfaces in Single-Component Systems. *Metall. Mater. Trans. A* **1995,** 26, 1917-1929.
39. Mullins, W. W. Theory of Thermal Grooving. *J. Appl. Phys.* **1957,** 28, 333-339.
40. Herring, C. Some Theorems on the Free Energies of Crystal Surfaces. *Phys. Rev.* **1951,** 82, 87-93.
41. Nichols, F. A.; Mullins, W. W. Surface (Interface) and Volume Diffusion Contributions to Morphological Changes Driven by Capillarity. *Trans. Metall. Soc. AIME* **1965,** 233, 1840-1845.
42. Combe, N.; Jensen, P.; Pimpinelli, A. Changing Shapes in the Nanoworld. *Phys. Rev. Lett.* **2000,** 85, 110-113.

43. Ekici, O.; Harrison, R. K.; Durr, N. J.; Eversole, D. S.; Lee, M.; Ben-Yakar, A. Thermal Analysis of Gold Nanorods Heated with Femtosecond Laser Pulses. *J. Phys. D: Appl. Phys.* **2008,** 41, 185501.
44. Taylor, A. B.; Chow, T. T. Y.; Chon, J. W. M. Alignment of Gold Nanorods by Angular Photothermal Depletion. *Appl. Phys. Lett.* **2014,** 104, 083118.
45. Gobel, H.; Von Blanckenhagen, P. A Study of Surface Diffusion on Gold with an Atomic Force Microscope. *Surf. Sci.* **1995,** 331, 885-890.
46. Ercolessi, F.; Andreoni, W.; Tosatti, E. Melting of Small Gold Particles: Mechanism and Size Effects. *Phys. Rev. Lett.* **1991,** 66, 911-914.
47. Miao, L.; Bhethanabotla, V. R.; Joseph, B. Melting of Pd Clusters and Nanowires: a Comparison Study using Molecular Dynamics Simulation. *Phys. Rev. B: Condens. Matter Mater. Phys.* **2005,** 72, 134109.
48. Antczak, G. y.; Ehrlich, G., *Surface Diffusion : Metals, Metal Atoms, and Clusters*. Cambridge University Press: New York, 2010.
49. Jiran, E.; Thompson, C. V. Capillary Instabilities in Thin-Films. *J. Electron. Mater.* **1990,** 19, 1153-1160.
50. Sun, H. T.; Yu, M. P.; Sun, X.; Wang, G. K.; Lian, J. Effective Temperature Sensing by Irreversible Morphology Evolution of Ultrathin Gold Island Films. *J.Phys Chem. C* **2013,** 117, 3366-3373.
51. Surrey, A.; Pohl, D.; Schultz, L.; Rellinghaus, B. Quantitative Measurement of the Surface Self-Diffusion on Au Nanoparticles by Aberration-Corrected Transmission Electron Microscopy. *Nano Lett.* **2012,** 12, 6071-6077.
52. Liu, M. Z.; Guyot-Sionnest, P.; Lee, T. W.; Gray, S. K. Optical Properties of Rodlike And Bipyramidal Gold Nanoparticles from Three-Dimensional Computations. *Phys. Rev. B* **2007,** 76, 235428.
53. Baierlein, R. The Elusive Chemical Potential. *Am. J. Phys.* **2001,** 69, 423-434.
54. Job, G.; Herrmann, F. Chemical Potential—a Quantity in Search of Recognition. *Eur. J. Phys.* **2006,** 27, 353-371.
55. Zijlstra, P.; Tchebotareva, A. L.; Chon, J. W. M.; Gu, M.; Orrit, M. Acoustic Oscillations and Elastic Moduli of Single Gold Nanorods. *Nano Lett.* **2008,** 8, 3493-3497.